Synthesis and characterization of low softening point high Bi_2O_3 glasses in the K_2O-B_2O_3-Bi_2O_3 system

Shiv Prakash Singh, Basudeb Karmakar*

Glass Science and Technology Section, Glass Division, Central Glass and Ceramic Research Institute (Council of Scientific and Industrial Research), 196, Raja S.C. Mullick Road, Kolkata 700032, India

Abstract

Synthesis of a new series of lead free low softening point (<470°C) high Bi_2O_3 (40-90 mol %) glasses in the K_2O-B_2O_3-Bi_2O_3 system by the melt-quench technique has been demonstrated here. Their structural, optical, thermal, electrical and other physical properties have been evaluated by X-ray diffraction (XRD), transmission electron microscopy (TEM), field emission scanning electron microscopy (FESEM), Fourier transformation infrared reflection spectroscopy (FTIRR), UV-Visible spectroscopy, dilatometer, LCR meter, etc. techniques. The glass softening point, glass transition temperature and glass deformation temperature are found to vary in the ranges 410-465°C, 354-409°C and 376-427°C respectively which are found to correlate well with the boron anomaly phenomenon (as revealed by FT-infrared reflection spectroscopy) with gradual addition of Bi_2O_3 in the glass matrix. The coefficient of thermal expansion shows a decreasing trend from 153 down to 109 x 10^{-7} K^{-1} whereas the dielectric constant increases from 21 to 34 with the increase in Bi_2O_3 content. The theoretical optical basicity is found to increase from 0.93 to 1.15 while the optical band gap decreases from 2.86 down to 2.30 eV with the addition of Bi_2O_3. The formation of metallic bismuth in these glasses during melting in air has been confirmed by the X-ray diffraction, transmission electron microscopy, selected area electron diffraction (SAED) and high resolution transmission electron microscopy (HRTEM) analyses. The formation of Bi_2O_3 rich secondary phase in the glasses and their particle size distribution has been examined by the field emission scanning electron microscopy photomicrograph analysis.

Keywords: Amorphous materials; Optical properties; Thermal expansion; X-Ray diffraction; Transmission electron microscopy

* Corresponding author. Tel.: +91 - 33 2473 3496: fax: +91 - 33 2473 0957.
E-mail: basudebk@cgcri.res.in (B. Karmakar).

1. Introduction

Recently, glasses containing bismuth have attained great attention, since they are used in the wide area of applications. The obtained glasses are characterized by high density, high refractive index and high dielectric constant properties. Hence there has been an increasing interest in the synthesis, microstructure and physical properties of heavy metal oxide (HMO) glasses containing bismuth as a major component. Bismuth oxide (Bi_2O_3) based glasses for their high polarizability has fascinated much attention of glass researchers because of their nonlinear optical properties which have importance for the development of optical information processing technology [1-3]. For this purpose, glasses of higher optical nonlinearity have to be found or designed on the basis of correlation of the optical nonlinearity with some other electronic properties which are easily understandable and accessible. Therefore, many studies on their structure and optical properties have been carried out. It has been found that glasses containing a large amount of Bi_2O_3 possess a wide range of infrared transparency [4-6]. Lead oxide is widely used as a component in the low melting glasses. But due to its hazardous effect on health and environment, it is being eliminated from various applications [7, 8]. In this context, bismuth oxide is a suitable substitute of lead oxide for its isoelectronic properties. Therefore, bismuth glasses are very useful for exploiting as lead-free high density radiation shielding window (RSW) glasses, as lead-free low-softening point dielectric glasses for plasma display panel, thick film conductors, sealing glasses for metals, etc. [7,8].

In addition to these, bismuth oxide glasses are very stable hosts for obtaining efficient luminescence in rare-earth ions. Recently, bismuth oxide glasses have attracted

much attention because of their low phonon energy. The quantum efficiency of emission from a given level strongly depends on the phonon energy of the host medium, it can be predicted that the nonradiative loss to the lattice vibration will be small and the fluorescence quantum efficiency will be high in bismuth oxide glasses. All these applications indicate the need of a basic understanding of the relationship among the electronic polarizability, optical basicity and optical properties of the bismuth oxide glasses.

Bismuth oxide cannot be considered as a glass network former due to small field strength (0.53) of Bi^{3+} ion. However, in combination with B_2O_3 glass former it is possible to obtain glasses in a relatively large compositional range. A survey of literature shows that there are many reports available on ternary bismuth borate glasses [9-14]. Saddeek [15] has reported about Li_2O-Bi_2O_3-B_2O_3 glass system. In this paper, we demonstrate the physical, structural, optical, thermal and electrical properties of a new series of glasses of high Bi_2O_3 content (40-90 mol %) in the K_2O-B_2O_3-Bi_2O_3 system.

2. Experimental Procedure

Bismuth trioxide, Bi_2O_3 (99%, Loba Chemie), boric acid, H_3BO_3 (99.5%, Loba Chemie) and potassium carbonate, K_2CO_3 (99.9%, Loba Chemie) were used as raw materials to prepare the glasses. The glass batch for 25 g glass of composition (100-x)(K_2O-B_2O_3)-xBi_2O_3 (mol %) (where x = 10, 20. 30, 40, 50, 60, 70, 80 and 90) was melted at 1100^oC in air for 30 min with intermittent stirring for 0.5 min in a 25 ml high purity silica crucible in an electrical furnace. The molten glass was cast into a carbon plate and annealed at 320^oC for 2h to release the internal stresses.

The softening point (T_s) of the samples was measured by a glass softening point system (Harrop/Labino, Model SP-3A) with an accuracy of $\pm 1^{o}$C. The instrument was previously calibrated with a NBS (National Bureau of Standards, USA) standard glass of known softening point. The coefficient of thermal expansion (CTE), glass transition temperature (T_g) and glass deformation temperature (T_d) of the cylindrical shaped glasses were measured with an accuracy of $\pm$0.2% using a horizontal-loading dilatometer (Netzsch, Model DIL 402 PC) after calibration with a standard alumina supplied with the instrument by the manufacturer. The coefficient of thermal expansion in the temperature range 50-300^{o}C is reported here. The dielectric constant was measured with an accuracy of $\pm$0.5% at a frequency of 1MHz using a LCR meter (Hioki, Model 3532-50 LCR Hitester) at 25^{o}C. The instrument was calibrated previously by a Suprasil-W silica glass (ε = 3.8). X-ray diffraction data of powder samples were recorded using an XPERTPRO diffractometer (PANalytical) with 2θ varying from 10^{o} to 80^{o} using Ni filtered CuKα (λ = 1.5406 *Å*) at 25^{o}C, generator power of 45 KV and 35 mA. Fourier transformation infrared reflection (FTIRR) spectra of polished glasses were recorded a by Perkin-Elmer Fourier transformation infrared reflection spectrometer (Model 1600) at a resolution of $\pm$ 2 cm^{-1} after 16 scans. The transmission electron microscopy (TEM) and selected area electron diffraction (SAED) images were taken using a FEI instrument (Tehnai-30, ST G^2) operating at an accelerating voltage of 200 kV. Field emission scanning electron microscopy (FESEM) photomicrographs were recorded with a Gemini Zeiss Supra™ 35VP Model (Carl Zeiss) instrument using an accelerating voltage of 4.9 kV. The sample was prepared for field emission scanning electron microscopy experiment by etching in 2 wt% of HF solution for 1 minute. The UV-Vis absorption spectra in the range of 300-

1100 nm were recorded using 2mm thickness of sample with a double beam UV-visible spectrophotometer (Lambda 20, Perkin-Elmer) at an error of $\pm$0.1 nm.

3. Results

3.1. Physical parameters

The samples containing 10, 20 and 30 mol% of Bi_2O_3 were not stable enough due to absorption of moisture from the environment, so characterizations of these samples were not possible. The other samples were prepared by cutting, grinding and polishing for various characterization measurements in various shapes. The glasses are labeled as KBB4, KBB5, KBB6, KBB7, KBB8 and KBB9 for x = 40, 50, 60, 70, 80 and 90 mol % of Bi_2O_3 content respectively.

The densities (ρ) of the glass samples were determined by the standard Archimedes principle. The measurements were done using single pan balance and distilled water as an immersion liquid. The density was obtained from the relation.

$$\rho = a\rho_x / (a-b) \qquad (1)$$

where a is the weight of the glass sample in air, b is the weight of the glass sample when suspended in distilled water (density of water, $\rho_x = 1 g.\ cm^{-3}$).

The molar volume (V_m) of the glass samples was calculated using the molecular weight (M) and density (ρ) of the glasses with the following relation and these values are also included in Table 1.

$$V_m = M/\rho \qquad (2)$$

The variation of density with the composition of Bi_2O_3 is shown in Table 1. It is evident from Table 1 that the density and molar volume of the glasses increase with increase in Bi_2O_3 content.

The refractive index (n) and Young's modulus were predicted using SciGlass (Glass Properties Information System, Version 6.7) software and these values are also listed in Table 1. Both these properties are found to increase with the increase in Bi_2O_3 content.

3.2. Optical transmission and absorption

Fig. 1 (a) shows the optical transmission spectrum of some glasses of the KBB system. The transmission of the glasses decreases with increase of Bi_2O_3 content. Figure 1 (b) shows the optical absorption bands of the glasses. Their surface plasmon resonance (SPR) absorption bands are also shown in the inset of Fig. 1 (b). The absorption coefficient, α near the edge of each curve was determined by using the following relation [16]

$$\alpha = 2.303A/t \qquad (3)$$

where A is absorbance and t is thickness of each sample. The relation between α and photon energy of the incident radiation, $h\nu$ is given by the following equation [12].

$$\alpha = B\,(h\nu - E_{opt})^2/h\nu \qquad (4)$$

where B is the constant and E_{opt} is the energy of the optical band gap. The relation (4) can be written as

$$(\alpha h\nu)^{1/2} = B(h\nu - E_{opt}) \qquad (5)$$

Using the relation (5) the optical band gap values were determined by the extrapolation of the linear region of the plots of $(\alpha h\nu)^{1/2}$ against $h\nu$. The values of E_{opt} thus obtained for all the glasses are given in the Table 1 and also shown in Fig. 2.

3.3. Theoretical optical basicity

The theoretical optical basicity (Λ_{th}) for the glass system under study has been calculated using the following relation [15-17].

$$\Lambda_{th} = X(K_2O)\,\Lambda(K_2O) + X(Bi_2O_3)\,\Lambda(Bi_2O_3) + X(B_2O_3)\,\Lambda(B_2O_3) \qquad (6)$$

where $X(K_2O)$, $X(Bi_2O_3)$ and $X(B_2O_3)$ are the equivalent fraction of the different oxides, i.e. the proportion of the oxide atom that contributes to the glass system; $\Lambda(K_2O)$, $\Lambda(Bi_2O_3)$ and $\Lambda(B_2O_3)$ are the optical basicity values of the constituent oxides. Here the values of $\Lambda(K_2O)$ = 1.4, $\Lambda(Bi_2O_3)$ = 1.19, $\Lambda(B_2O_3)$ = 0.425 have been taken from the literature [18]. The calculated values of Λ_{th} are presented in Table 1.

3.4. X-ray diffraction (XRD) pattern

Figure 3 shows the X-ray diffraction patterns of characteristic crystalline phases in KBB5 and KBB9 glass samples. The XRD peaks are not well resolved and are depict at $2\theta = 12.49^o$, 27.53^o and 28.50^o.

3.5. Transmission electron microscopy (TEM)

The TEM images of the KBB5 and KBB9 glasses are shown in Figs. 4 and 5 respectively. The average particle size of KBB5 glass is about 5 nm whereas that of KBB9 glass ranges 5 – 17 nm. Their respective selected area electron diffraction (SAED)

patterns show incipient crystalline behavior of the glasses. KBB5 shows <024> hkl plane and KBB9 depicts <024> and <208> diffraction hkl planes of rombohedral metallic bismuth (JCPDS File Card No.: 85-1329). The high resolution transmission electron microscopy (HRTEM) of KBB9 glass reveals <015> hkl planes of rombohedral metallic bismuth which has been identified from the d-spacing as provided in the JCPDS File Card No.: 85-1329. The TEM images of KBB9 glass show the presence of spherical as well as elongated particles in the glasses.

3.6. Field emission scanning electron microscopy (FESEM) micrograph

Figures 6 (a) and (c) show the FESEM micrographs of phase separation in glass samples KBB5 and KBB9 respectively. The FESEM image of KBB9 reveals the relatively dense and bigger size particles in comparison to KBB5 glass sample. The distribution of different size of phase separated particles is shown in the form of histograms with the respective micrographs in Fig. 6 (b) and (d) respectively. The KBB9 shows wide range of particle size ranges from 30 to 210 nm whereas the sample of KBB5 glass shows the particles of sizes ranges from 30 to 170 nm. The median size of particles is 80 nm for KBB5 where as it is 90 nm for KBB9. So it is seen that the median particle size and number of particles per unit area increase with the increase in Bi_2O_3 content. The number density of particles per unit area has been calculated for the both samples and found to be 12,985 and 13,149 particles/μm^2 for KBB5 and KBB9 glasses respectively.

3.7. FTIRR spectra

The infrared reflection spectra recorded for all the glass samples are shown in the Fig. 7 (a). The glass samples show bands at 451, 882, 1180 and 1265 cm^{-1}. A shoulder at around 707 cm^{-1} is also observed in the glasses. The reflection intensity ratio of BO_4 to BO_3 structural units is also demonstrated in the Fig. 7 (b). The values of the ratio of the two structural units of borate is gradually going down to 60 mol % of Bi_2O_3 content (KBB6) and then going up to 90 mol % of Bi_2O_3 content (KBB9) glasses. This observation reveals the boron anomaly phenomenon in these glasses.

3.8. Coefficient of thermal expansion (CTE)

The thermal expansion is a very important thermal property of glass. Fig. 8 (a) shows the linear thermal expansion of the KBB4, KBB7 and KBB9 glasses as a function of temperature. The variation coefficient of thermal expansion (CTE) of the glasses measured from 50 to 300^oC temperature range is shown in the Fig. 8 (b) as a function of Bi_2O_3 content. The CTE values vary from 153 to 109 x 10^{-7} K^{-1}. The CTE gradually decreases as Bi_2O_3 content increases form 40 to 90 mol%. However, these values deviate from the linearity in Bi_2O_3 content.

3.9. Softening point, glass transition temperature and deformation temperature

The softening point (T_s), glass transition (T_g) and deformation temperature (T_d) are shown in the Fig. 9. The values of these properties gradually going down as the Bi_2O_3 content increases from 40 to 60 mol% and further going up with Bi_2O_3 content increases

from 70 to 90 mol%. The (T_s), (T_g) and (T_d) are shown the lowest values at 60 mol% of Bi_2O_3 content i. e. in glass KBB6.

3.10. Dielectric constant

Dielectric constant (ε) of the glasses have been calculated by using the following formula [19]

$$\varepsilon = cd/(0.0885\ A) \quad (7)$$

where *c*, *d* and *A* are capacitance in pico Farad (*pF*), thickness of glass (in *cm*) and area of the dielectric (in cm^2) respectively.

It is seen that the dielectric constant of the glasses gradually increases with increase in Bi_2O_3 content which is shown in the Fig. 10. Dielectric constant (ε) is associated with polarizability (α_p) and refractive index (n) by the following Lorentz-Lorenz (Eq. 8) and Maxwell equations (Eq. 9) [20].

$$\alpha_p = 3M_{av}\,(n^2 - 1)/4(n^2 + 2)\pi N_A \rho \quad (8)$$

$$\varepsilon = n^2 \quad (9)$$

where N_A is the Avogadro's number, and M_{av} and ρ are average molecular weight and density of the glass respectively.

4. Discussion

In this study of K_2O-B_2O_3-Bi_2O_3 ternary glass system, the replacement of Bi_2O_3 instead of B_2O_3 and K_2O increases the density. This is attributed to the replacement of low density oxides (B_2O_3 and K_2O) by high density oxide (Bi_2O_3) as shown in Table 1. The molar volume (V_m) of the glasses increases due to increase in bond length or inter

atomic spacing. It has happened due to higher ionic radius of Bi^{3+} (0.102 nm) than that of B^{3+} (0.020 nm). Therefore, one can understand that V_m as the volume corresponding structural unit with its surrounding space will increase by insertion of HMO like bismuth oxide.

The optical band gap (E_{opt}) of the samples decrease to lower energies with increase in Bi_2O_3 content. It is related to the progressive increase in the covalent Bi-O of bond strength of 81.9 kcal mol^{-1} [13]. This increased Bi_2O_3 content gives rise to possible decrease in the B-O-B bridging oxygen of borate structural unit. Here it is believed that as the cation concentration increases which developed the bridging oxygen bonds with Bi^{3+} ion and lead to the gradual breakdown of the glass network. This incident seems to account for the decrease in the E_{opt} value, which results in the shifting of edge to longer wavelength with increase in Bi_2O_3 content from 40 to 90 mol %. Such a decrease in the values of optical band gap energy can thus be attributed to decrease in the phonon-assistant indirect transitions.

It is observed from the Table 1 that the theoretical optical basicity (Λ_{th}) values increases with increase in Bi_2O_3 content. This may be understood according to Eq. (6). It is well known that Bi^{3+} ions are highly polarizable ion [21], so the polarizability of the glasses is increases with the increase in Bi_2O_3 content. Therefore, it can be concluded that the basicity increases with the increase in the polarizability as Bi_2O_3 content gradually increases.

The XRD patterns show the peaks for the 012, 116 and 122 Miller planes of the rhombohedral metallic bismuth phase (JCPDS file no. 01-0699) in the Fig. 3. The bismuth glasses are dark brown or black colored when at high melting temperature and

contain high Bi_2O_3. Sanz *et al.* [9] and Zhang *et al.* [10] have found these crystalline peaks for metallic bismuth in deep brown colored bismuth glasses which are reduced during melting process. The reduction reaction can be represented by

$$Bi_2O_3 \rightleftharpoons 2Bi^o + 3/2\ O_2 \qquad (10)$$

The above result also confirmed from the TEM images of KBB5 and KBB9 glasses (Figs. 4 and 5 respectively). It clearly reveals that the KBB9 glass has homogeneously dispersed Bi^o nanoparticles (NPs) of spherical shape with bigger size than that of KBB5 glass. This observation also confirm from the SAED pattern of KBB9 glass which shows the more distinct spots than that of KBB5 glass due to its bigger particle size. The KBB9 glass also depicts the lattice fringes of metallic bismuth in HRTEM which is not found in KBB5 glass due to its small size. This formation of more and bigger particle in KBB9 glass is also supported by the optical transmission spectra (Fig. 1 (a)). The gradual decrease in transmittance from KBB5 to KBB9 glasses along the visible spectrum is due to the existence of more metallic bismuth particles dispersed in the KBB9 glass.

The UV-Vis absorption spectra of bismuth glasses in Fig. 1 (b) show the absorption bands of the surface plasmon resonance (SPR) of Bi^o nanoparticles (NPs). Khonthon *et al.*[4] has reported the SPR band of Bi^o NPs at 460 nm, which are comparable to our results. The absorption bands shift towards higher wavelength with the increase in Bi_2O_3 content. The SPR of a metal particle gives an absorbance band centered at a wavelength, λ, which can be expressed by the relation: [22]

$$\lambda^2 = (2\pi c)^2 \varepsilon_o m_o (\varepsilon_\infty + 2n^2) / Ne^2 \quad (11)$$

where the velocity of light is c, m_o is the particle mass, N is the particle concentration, the charge of the electron is e, ε_∞ is the optical dielectric function of the metal, n is the refractive index of the host material and ε_o is the free-space permeability. From the Eq. 11, it is clear that the position and shape of the SPR is determined by the metal dielectric function, as well as on the size and shape of the particles, refractive index of the host materials and concentration of particles. The SPR band of Bi^o NPs in the host water (refractive index, n = 1.33) was observed around 400 nm [23] whereas here the glasses having higher refractive index (2.02 – 2.43) show a red shift towards higher wavelength of the band. The two spectrally separated absorption bands of glasses (Fig. 1 (b)) indicate that the two groups of size (small and large) and shape (elongated) of particles are present in the glasses. These findings can be correlated well with the TEM images (Figs. 4 and 5) where both small and big size particles are present. Fig. 5 shows the presence of some spherical as well as elongated shaped particles in the glass. The spherical particles generate a single SPR band, which is located in the visible range, whereas elongated particles give rise to two spectrally separated SPR bands corresponding to transverse and longitudinal electron oscillations with respect to major axis [24].

Fig. 6 shows the FESEM micrograph of KBB5 and KBB9 glasses. These micrographs indicate the phase separation in the glass. Scholze [20] has explained this type of phase separation is a very common phenomenon in the glass because during melting process all components are in liquid phase. During quenching any of the

components get supersaturation state and form a separated secondary phase. Porai-Koshits *et al.* [25], W. Vogel *et al.* [26], James *et al.* [27] and MacDowell *et al.* [28] have worked on the phase separation in various glasses. Porai-Koshits *et al.* [25] have report about such fine structure of sodium silicate glasses arises due to the secondary phase separation from a primary separated phase take place as a result of over saturation under the lowering of temperature during the process of quenching. W. Vogel *et al.* [26] has done electron microscopical studies of phase separated glasses. MacDowell *et al.* [28] has observed metastable glass in glass separation on rapid quenching of Al_2O_3-SiO_2 glass melt. Here in this study, Fig. 6 depicts the secondary phase in the K_2O-Bi_2O_3-B_2O_3 glass system. During etching process by HF solution at the time of sample preparation for the FESEM experiment the B_2O_3 and K_2O were rapidly dissolved. Therefore the observed micro images are due to Bi_2O_3 rich phase. This can also be concluded from the evidence of increasing the number of particles in the observed micrograph images with the Bi_2O_3 content.

Bi_2O_3 containing glasses have fundamental vibrations in the IR spectral regions at around 480, 715 and 880 cm^{-1} [29, 30]. Boron also has three vibrational bands at 1200-1600, 800-1200 and 700 cm^{-1} [29-34]. The boron-oxygen network can be in the form of planar BO_3 or tetrahedral BO_4. The Fig. 7 (a) shows reflection bands at 451 cm^{-1}, specific to the vibrations of Bi–O bonds in BiO_6 octahedral units [29, 30]. The absorption band at 707 cm^{-1} has been assigned to symmetric stretching vibrations of Bi–O bonds in BiO_3 pyramidal units [29, 30]. The band at 882 cm^{-1} is due to stretching vibration of the B–O bonds in tetrahedral BO_4 unit and the broad band at 1180 and 1265 cm^{-1} is attributed to the B–O bond stretching in the planar BO_3 unit in the borate network [29-34]. This

bifurcation is due to the bridging of BO_3 with K-O and Bi-O units. This bifurcation gradually weakens with the increase in the content of Bi_2O_3 which indicates the major bridging of BO_3 unit with the Bi-O. From Fig. 7 (a), it seen that the Bi_2O_3 act as modifier at lower concentration and modify the glass structure by breaking the B-O bond and form the Bi-O of the BiO_3 unit which exhibited the band at 707 cm^{-1}. But at higher concentration of Bi_2O_3, it acts as a glass former and form Bi-O of BiO_6 octahedral units. Fig. 7 (b) shows the variation of BO_4 and BO_3 structural units of borate which indicates the tetrahedral BO_4 decreases upto KBB6 and further increases at higher concentration of Bi_2O_3. Scholze [20] has explained this anomaly property of boron due to shifting of coordination number (CN) from BO_4 (CN = 4) to BO_3 (CN = 3) and again to BO_4 structural units. The planar structure of BO_3 group weakens the glass network whereas tetrahedral BO_4 unit strengthen the network. Duffy [17] has also reported the major structural changes in certain properties due to boric oxide anomaly.

The thermal expansion of glasses is controlled by the asymmetry of the amplitude of thermal vibrations in the glass. It decreases as the rigidity of the glass network increases [35]. An increase of the number of non-bridging bonds weakens the structure which is turn increases the coefficient of thermal expansion, whereas the change in coordination number of network former cation may cause either its increase or decrease depending on the effect on glass structure. In this study, coefficient of thermal expansion gradually decreases with the increase in the Bi_2O_3 content in the glasses which is shown in the Fig. 8 (a). Here the Bi^{3+} substituting B^{3+} form the BiO_6 octahedral units with coordination number six. Therefore, the coordination number of cation has changed from 4 or 3 (BO_4 or BO_3 structural unit) to 6 (BiO_6 structural unit). The anomaly tendency of

the thermal expansion shown by dotted line in Fig. 8 (b). This could also be well correlated with the ratio of BO_4 to BO_3 structural unit formation (see Fig. 7 (b)).

Fig. 9 shows softening point (T_s), glass transition temperature (T_g) and glass deformation temperature (T_d) decreases from 40 to 60 mol% and subsequently increase with higher concentration of Bi_2O_3. The Bi_2O_3 act as a glass network modifier at low concentration where as it form network by itself at high concentration [13]. The decrease in the values of above properties is due to the increase in number of non-bridging oxygens (NBOs) atoms with the increasing concentration of Bi_2O_3. Addition of lower concentration of Bi_2O_3 as a third component into the binary potassium borate glasses results in splitting of K-O-K and B-O-B bonds and hence the bridging oxygens (BOs) are converted into NBOs. Further addition of Bi_2O_3 into glass opens up the glass network. This results in weakening of the glass network. Hence the softening point, glass transition temperature and glass deformation temperature decrease up to 60 mol % of Bi_2O_3 content as shown in the Fig. 9. It is obvious that the decreases in the above values are due to increase in the number of Bi-O which are weaker than B-O linkages. It may be noted that the bond strength of Bi-O is 81.9 kcal mol^{-1} which is less than that of B-O (192.7 kcal mol^{-1}) [13]. But the values of T_s, T_g and T_d further increases at higher concentration (70 to 90 mol %). Here it can be noted that at higher concentration, Bi_2O_3 acts as a glass network former by reshuffling the glass network. It form Bi-O bond of BiO_6 octahedral unit and again rebuild the structure by Bi-O-Bi, hence the rigidity of the glasses increases. Therefore, the values of above properties increase at higher concentration of Bi_2O_3. These phenomena correlate well with the ratio of I_{BO4}/I_{BO3} as shown in Fig. 7 (b) which shows the boron anomaly property in these glasses as well.

The dielectric constant is directly correlated with the polarizability of the samples. The dielectric constant gradually increases with the increase in the Bi_2O_3 content in the glasses which is shown in the Fig. 10. It has already been reported that Bi^{3+} ions are highly polarizable (above 3 $A^{\circ 3}$) due to their large ionic radii and small cation unit field strength [13, 21]. The observation made from Table 1 is that the refractive index also increases with the increase of bismuth oxide content. Eqs. 9 and 10 also disclose the increasing trend of dielectric constant with increase in Bi_2O_3 content. This is due to the high ionic refraction of Bi^{3+} ion (30.5) [36].

5. Conclusions

The effect of the Bi_2O_3 content on the properties of the glasses in the K_2O- B_2O_3-Bi_2O_3 system has been investigated here. The densities and molar volume of the glasses increase due to the incorporation of Bi_2O_3. The transmission and optical band gap energy going down as bismuth oxide content increases. The SPR bands, XRD patterns, TEM images and SAED confirm the formation of nanometal of bismuth during melting. They also reveal that the metallic bismuth particle size gradually increases at higher Bi_2O_3 in the glass composition. The TEM images revealed that the particles are present in the glasses are both in small and big sizes having spherical as well as elongated shape. This is also supported by SPR absorption bands which show two spectrally separated bands. The FESEM microstructure of the glasses shows the bismuth oxide rich secondary phase separation in the glass. Addition of Bi_2O_3 in the glass facilitates the formation of BiO_6 octahedral unit by replacing B-O bond. The glasses exhibit the boron anomaly phenomena. The decrease in the values of glass softening temperature, glass transition

temperature and glass deformation temperatures from 40 to 60 mol % of Bi_2O_3 indicates that the glass network becomes less tightly packed due to formation of nonbridging oxygen. But these values are further increased with Bi_2O_3; this reveals the role of Bi_2O_3 as a glass network former at its higher concentration. These results correlate well with the FTIRRS reflection intensity ratio of the BO_4 to BO_3 structural units. The basicity and polarization of the samples have increased with the bismuth oxide content which causes the increase in dielectric constant. This rise in the dielectric constant is also correlated well with the increase in refractive index of the glasses. We believe that this work will create new prospect in the area of lead-free low-softening point glasses.

Acknowledgements

SPS express his sincere gratitude to the financial support of the Council of Scientific and Industrial Research (CSIR), New Delhi in the form of CSIR-SRF under sanction number 31/15(78)/2010-EMR-I. The authors thank Prof. Indranil Manna, Director of the institute for his kind permission to publish this paper. The technical supports obtained from the infrastructural facilities (XRD and Electron Microscope Divisions) of this institute are also thankfully acknowledged.

References

[1] Zhou S, Jiang N, Zhu B, Yang H, Ye S, Laksminarayana G, Hao J, Qiu J. Multifunctional bismuth-doped nanoporous silica glass: from blue-green, orange, red, and white light sources to ultra-broadband infrared amplifiers. Adv Funct Mater 2008; 18: 1407.

[2] Meng X, Qiu J, Peng M, Chen D, Zhao Q, Jiang X, Zhu C. Infrared broadband emission of bismuth-doped barium-aluminum-borate glasses. Optics Exp 2005; 13: 1635.

[3] Wang Y, Dai S, Chen F, Xu T, Nie Q. Physical properties and optical band gap of new tellurite glasses within the TeO_2–Nb_2O_5–Bi_2O_3 system. Mater Chem Phys 2009; 113: 407.

[4] Khonthon S, Morimoto S, Arai Y, Ohishi Y. Redox equilibrium and NIR luminescence of Bi_2O_3-containing glasses. Opt Meter 2009; 31: 1262.

[5] Peng M, Chen D, Qui J, Jiang X, Zhu C. Bismuth doped zinc aluminosilicate glasses and glass-ceramics with ultra-broadband infrared luminescence. Opt Mater 2007; 29: 556.

[6] Ren J, Dong G, Xu S, Bao R, Qiu J. Inhomogeneous broadening, luminescence origin and optical amplification in bismuth-doped glass. J Phys Chem A 2008; 112: 3036.

[7] An J-S, Park J-S, Kim J-R, Hong KS. Effects of Bi_2O_3 and Na_2O on the thermal and dielectric properties of zinc borosilicate glass for plasma display panels. J Am Ceram Soc 2006; 89: 3658.

[8] Hrovat M, Maeder T, Holc J, Belaviˇc D, Cilenˇsek J, Bernard J. Subsolidus phase equilibria in the RuO_2–Bi_2O_3–SiO_2 system. J Euro Ceram Soc 2008; 28: 2221.

[9] Sanz O, Haro-Poniatowski E, Gonzalo J, Navarro JMF. Influence of the melting conditions of heavy metal oxide glass contaning bismuth oxide on their optical absorption. J Non-Cryst Solids 2006; 352: 761.

[10] Zhang Y, Yang Y, Zheng J, Hua W, Chen G. Effects of oxidizing additives on optical properties of Bi_2O_3-B_2O_3-SiO_2 glasses. J Am Ceram Soc 2008; 91: 3410.

[11] Sun H, Wen L, Xu S, Dai S, Hu L, Jiang Z. Novel Litthium-Barium-Lead-Bismuth Glasses. Mater Lett 2005; 59: 959.

[12] Lee S, Hwang S, Cha M, Shin H, Kim H. Role of copper ion in preventing silver nanoparticles forming in Bi_2O_3-B_2O_3-ZnO glass. J Phys Chem Solids 2008; 69: 1498.

[13] Saritha D, Markandeya Y, Salagram M, Vithal M, Singh AK, Bhikshamaiah G. Effect of Bi_2O_3 on physical, optical and structural studies of ZnO-Bi_2O_3-B_2O_3 glasses. J Non-Cryst Solids 2008; 354: 5573.

[14] Qiu HH, Ito T, Sakata H. DC conductivity of Fe_2O_3–Bi_2O_3–B_2O_3 glasses. Mater Chem Phys 1999; 58: 243.

[15] Saddeek YB, Ultrasonic study and physical properties of some glasses. Mater Chem Phys 2004; 83: 222.

[16] Dimitrov V, Komatsu T. Classification of oxide glasses: a polarizability approach. J Solid State Chem 2005; 178: 831.

[17] Duffy JA. The refractivity and optical basicity of glass. J Non-Cryst Solids 1986; 86: 149.

[18] Duffy JA. Ingram MD. Optical Properties of Glass. Westerville: The American Ceramic Society, 1991. p. 159-184.

[19] Dakin TK. Standard Handbook for Electrical Engineers. New York: McGraw Hill Inc, 1993. p. 4-117-130.

[20] Scholze H. Glass, Nature, Stucture and Properties, 3rd edition. New York: Springer, 1991.

[21] Zhao X, Wang X, Lin H, Wang Z. Correlation among electronic polarizability, optical basicity and interaction parameter of Bi_2O_3-B_2O_3 glasses. Physica B 2007; 390: 293.

[22] Persans PD, Stokes KL. Handbook of Nanophase materials. New York: Marcel Dekker, 1997. p. 271.

[23] Gonella F, Mazzoldi P. Handbook of Nanostructured Materials and Nanotechnology, **Vol. 4.** London: Academic Press, 2000. p. 81-101.

[24] Kreibig U, Vollmer M. Optical Properties of Metal Clusters. Berlin: Springer, 1995.

[25] Porai-Koshits EA, Averjanov VI. Primary and secondary phase separation of sodium silicate glasses. J Non-Cryst Solids, 1968; 1: 29.

[26] Vogel W, Horn L, Reiss H, Volksch G. Electron-microscopical studies of glasses. J Non-Cryst Solids 1982: 49: 221.

[27] James PF, Quantitative measurements of phase separation in glasses using transmission electron microscopy. part I. experimental technique and method of analysis. McMillan PW. Phys Chem Glasses 1970; 11: 59.

[28] MacDowell JF, Beall GH. Immiscibility and crystallization in Al_2O_3-SiO_2 glasses. J Am Ceram Soc 1969; 52: 17.

[29] Doweidar H, Saddeek YB. FTIR and ultrasonic investigation on modified bismuth borate glasses. J Non-Cryst Solids 2009; 355: 348.

[30] Ardelean I, Cora S, Rusu D. EPR and FT-IR spectroscopic studies of Bi_2O_3-B_2O_3-CuO glasses. Physica B 2008; 403: 3682.

[31] Fuxi G. Optical and Spectroscopic properties of Glass, Berlin: Springer-Verlag, 1992.

[32] Kamitsos EI, Karakassides MA, Chryssikos GD. Vibrational spectra of magnesium-sodium-borate glasses. 2. raman and mid-infrared investigation of the network structure. J Phys Chem 1987; 91: 1073.

[33] Kharlamov AA, Almeida RM, Heo J. Vibrational Spectra and Structure of Heavy Metal Oxide Glasses. J Non-Cryst Solids 1996; 202: 233.

[34] Motke SG, Yowale SP, Yawale SS. Infrared spectra of zinc doped lead borate glasses. Bull Mater Sci 2002; 25: 75.

[35] Gavriliu G. Thermal expansion and characteristic points of $–Na_2O–SiO_2$ glass with added oxides. J Euro Ceram Soc 2002; 22: 1375.

[36] Volf MB. Chemical Approach to Glass, Amsterdam: Elsevier, 1984.

Figure captions

Fig. 1. (a) Transmission and (b) absorbance spectra of (1) KBB4, (2) KBB5, (3) KBB6 and (4) KBB9 glasses. Their surface plasmon resonance (SPR) absorption bands are shown in inset of (b).

Fig. 2. Plot of $(\alpha h\nu)^{1/2}$ as a function of photon energy ($h\nu$) for KBB4, KBB5, KBB6, KBB7, KBB8 and KBB9 glasses.

Fig. 3. XRD patterns of (a) KBB5 and (b) KBB9 glasses.

Fig. 4. TEM image and SAED pattern of KBB5 glass.

Fig. 5. TEM images of KBB9 glass (a) and (b). Its HRTEM and SAED pattern are in (c) and (d) respectively.

Fig. 6. (Color online) FESEM micrographs of (a) KBB5 and (c) KBB9 glasses show the effect of Bi_2O_3 content on the phase separated particle size distribution which is plotted in (b) and (d) respectively (where R is the correlation coefficient).

Fig. 7. (a) FTIRR spectra of (1) KBB4, (2) KBB5 (3) KBB6, (4) KBB7, (5) KBB8 and (6) KBB9 glasses and (b) variation of reflection intensity ratio of BO_4 to BO_3 structural units of the glasses as a function of Bi_2O_3 content.

Fig. 8. (a) Linear thermal expansion of (1) KBB4, (2) KBB7 and (3) KBB9 glasses as a function of temperature. Their T_g and T_d values are also shown and (b) variation of coefficient of thermal expansion (CTE) of the glasses as a function of Bi_2O_3 content.

Fig. 9. Variation of softening temperature (T_s), glass transition temperature (T_g) and deformation temperature (T_d) of the glasses as a function of Bi_2O_3 content.

Fig. 10. Variation of dielectric constant of the glasses as a function of Bi_2O_3 content.

Table 1
Some experimental and calculated properties of the glasses in the K_2O-B_2O_3-Bi_2O_3 system

Property	KBB4	KBB5	KBB6	KBB7	KBB8	KBB9
Density, ρ (g. cm^{-3}) ($\pm$ 0.01)	5.076	5.625	6.133	6.496	6.723	6.946
Optical band gap energy, E_{opt} (eV) ($\pm$0.1)	2.86	2.78	2.69	2.59	2.50	2.30
Average molecular weight, M_{av}	235.53	273.93	312.34	350.74	389.15	427.55
Molar volume, V_m (cm^3) ($\pm$0.01)	46.40	48.70	50.93	53.33	58.98	61.55
Theoretical optical basicity, Λ_{th}	0.93	0.98	1.03	1.08	1.12	1.15
Refractive index, n	2.024	2.142	2.220	2.294	2.366	2.434
Young's modulus (GPa)	42.96	49.17	53.70	58.03	62.19	66.17

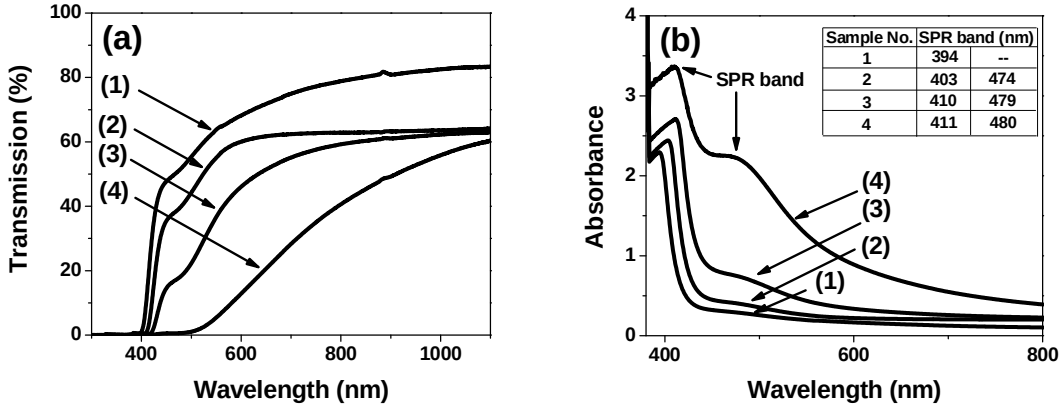

Fig. 1. (a) Transmission and (b) absorbance spectra of (1) KBB4, (2) KBB5, (3) KBB6 and (4) KBB9 glasses. Their surface plasmon resonance (SPR) absorption bands are shown in inset of (b).

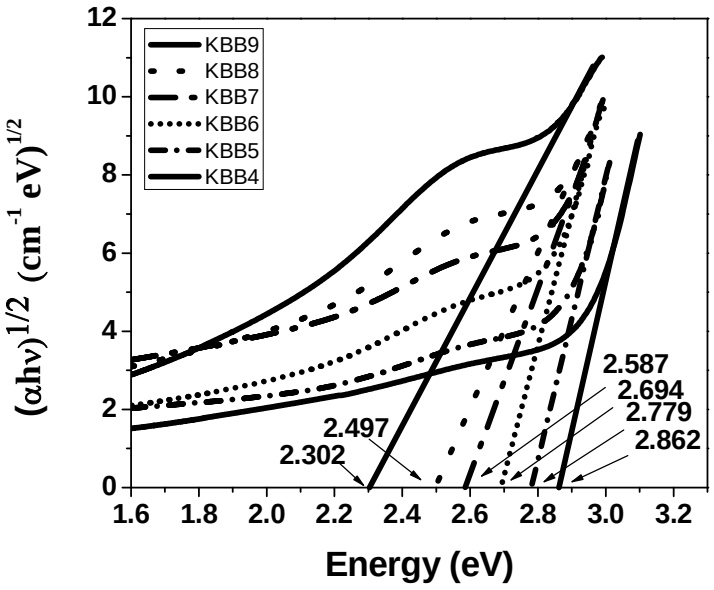

Fig. 2. Plot of $(\alpha h\nu)^{1/2}$ as a function of photon energy ($h\nu$) for KBB4, KBB5, KBB6, KBB7, KBB8 and KBB9 glasses.

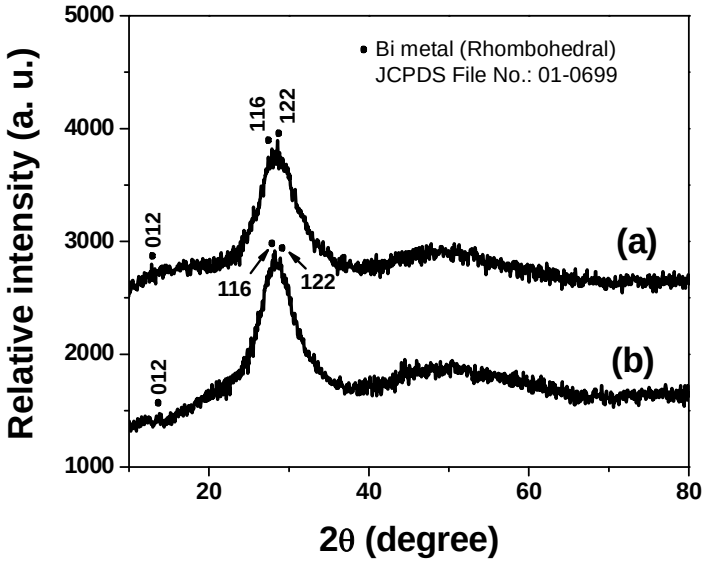

Fig. 3. XRD patterns of (a) KBB5 and (b) KBB9 glasses.

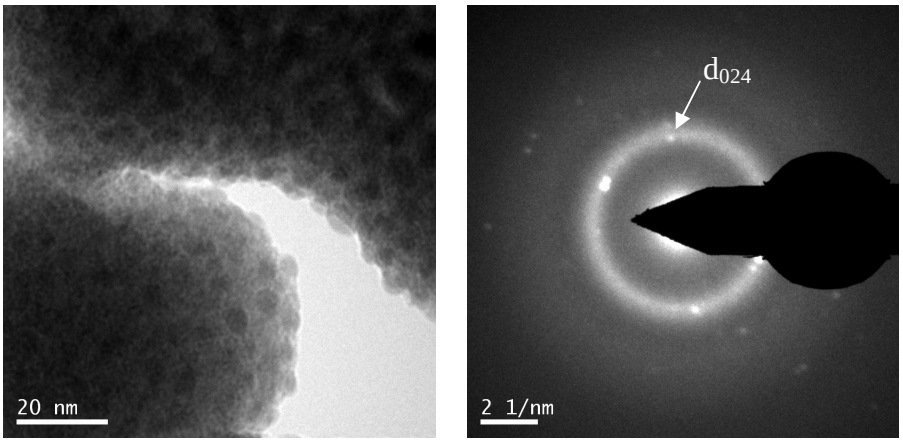

Fig. 4. TEM image and SAED pattern of KBB5 glass.

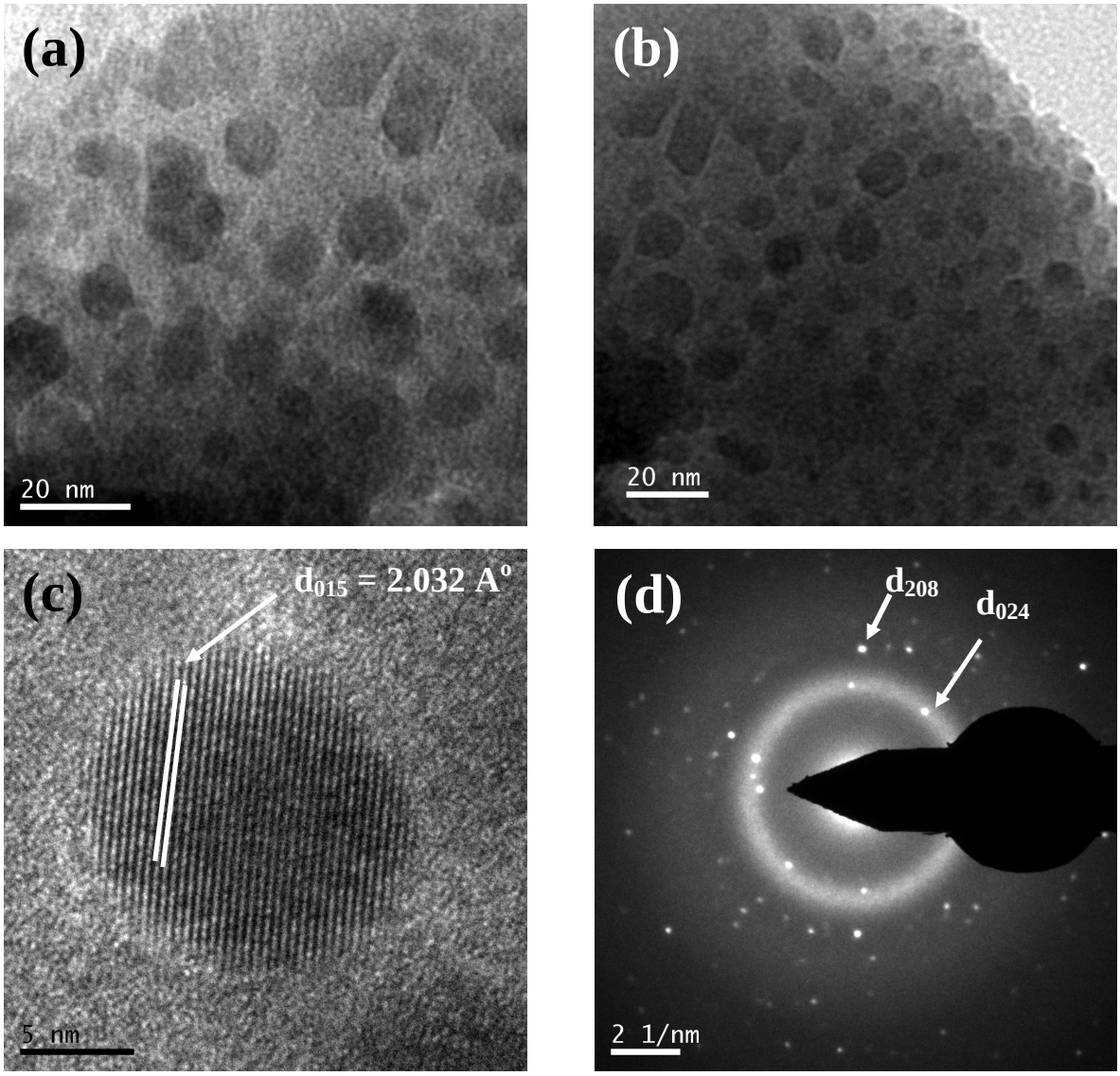

Fig. 5. TEM images of KBB9 glass (a) and (b). Its HRTEM and SAED pattern are in (c) and (d) respectively.

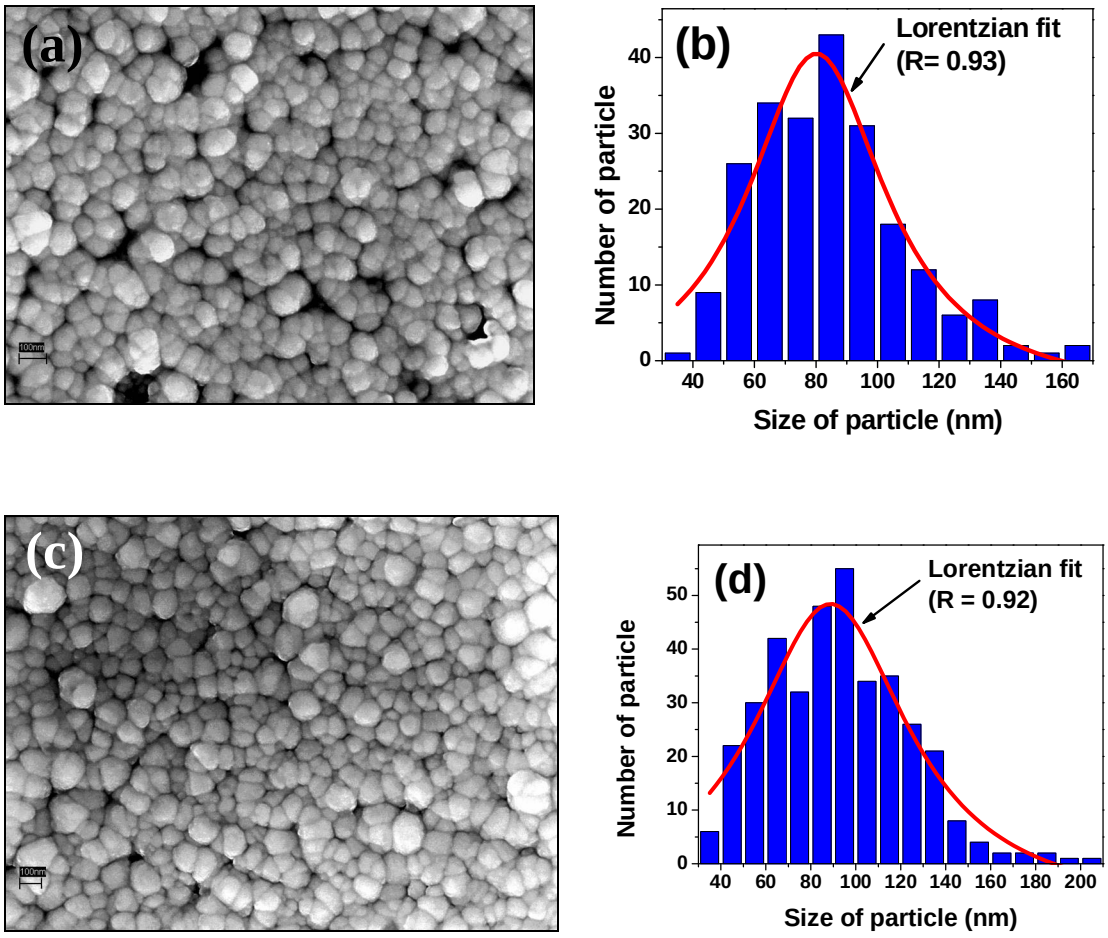

Fig. 6. (Color online) FESEM micrographs of (a) KBB5 and (c) KBB9 glasses show the effect of Bi_2O_3 content on the phase separated particle size distribution which is plotted in (b) and (d) respectively (where R is the correlation coefficient).

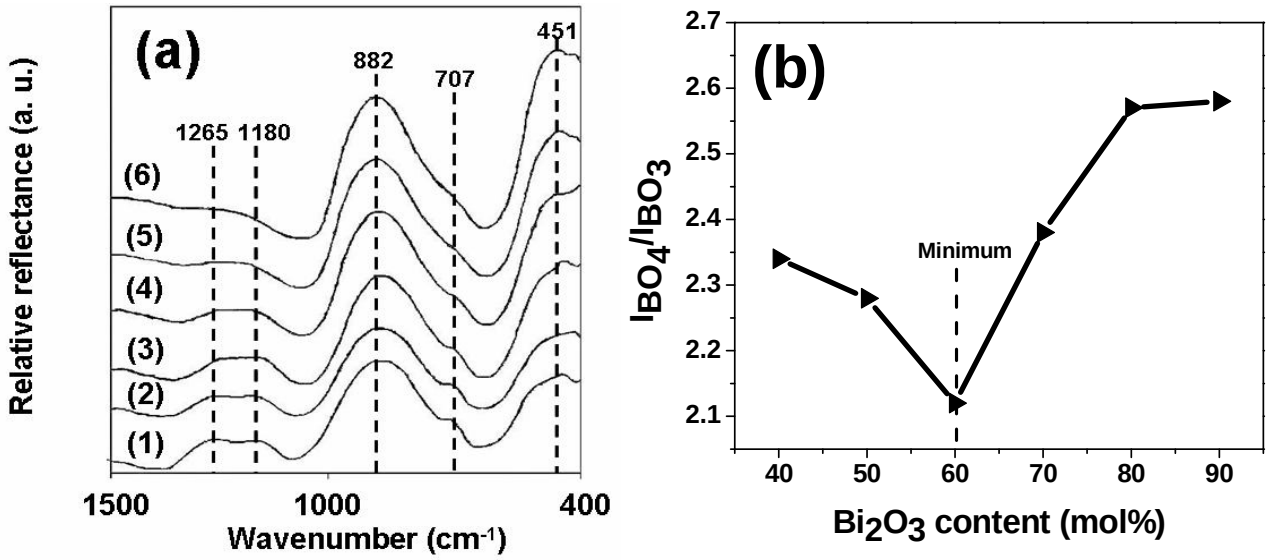

Fig. 7. (a) FTIRR spectra of (1) KBB4, (2) KBB5 (3) KBB6, (4) KBB7, (5) KBB8 and (6) KBB9 glasses and (b) variation of reflection intensity ratio of BO_4 to BO_3 structural units of the glasses as a function of Bi_2O_3 content.

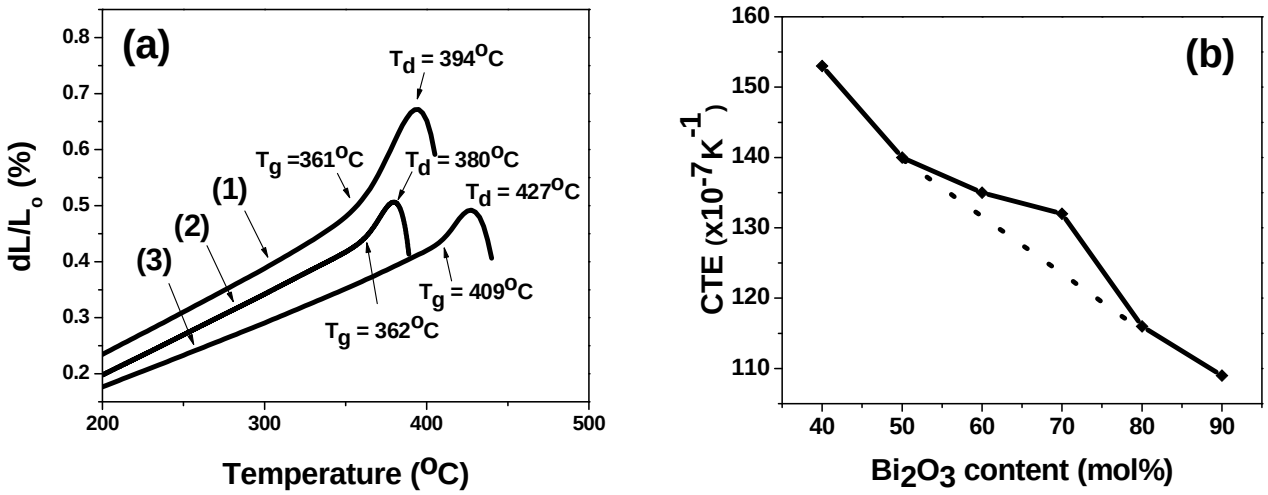

Fig. 8. (a) Linear thermal expansion of (1) KBB4, (2) KBB7 and (3) KBB9 glasses as a function of temperature. Their T_g and T_d values are also shown and (b) variation of coefficient of thermal expansion (CTE) of the glasses as a function of Bi_2O_3 content.

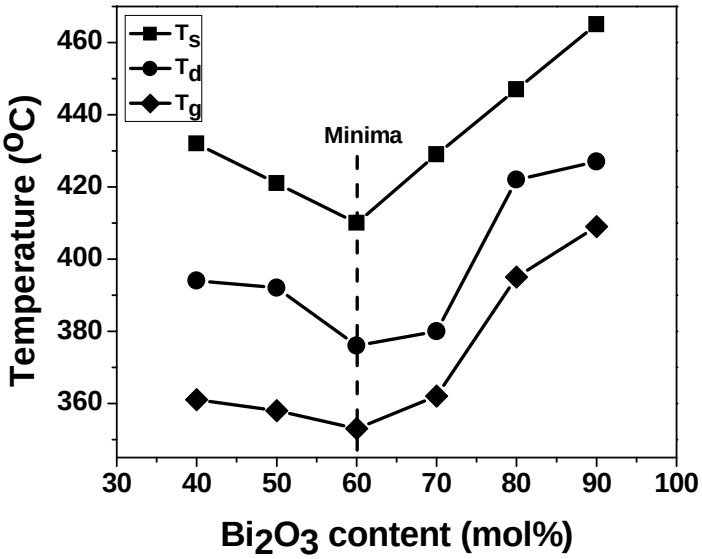

Fig. 9. Variation of softening temperature (T_s), glass transition temperature (T_g) and deformation temperature (T_d) of the glasses as a function of Bi_2O_3 content.

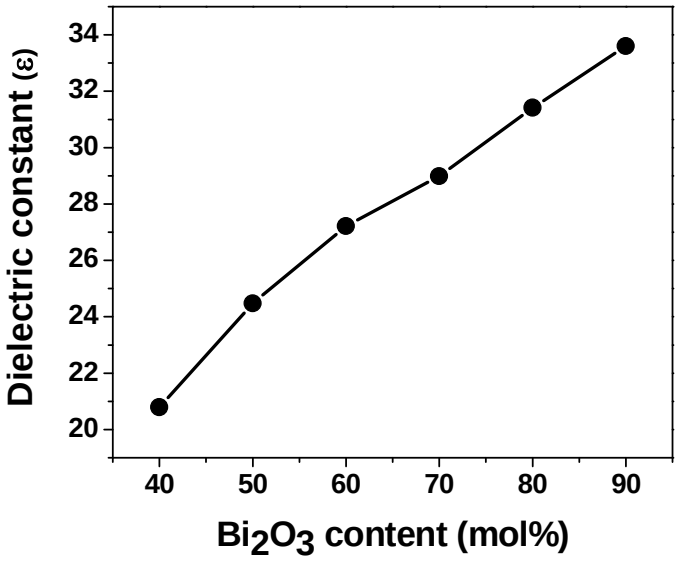

Fig. 10. Variation of dielectric constant of the glasses as a function of Bi_2O_3 content.